Solid State Ionics 184 (2011) 52–56

Contents lists available at ScienceDirect

Solid State Ionics

journal homepage: www.elsevier.com/locate/ssi

Potential energy landscapes for anion Frenkel-pair formation in ceria and india

Aron Walsh *, Scott M. Woodley, C. Richard A. Catlow, Alexey A. Sokol

University College London, Department of Chemistry, Materials Chemistry, 3rd Floor, Kathleen Lonsdale Building, Gower Street, London WC1E 6BT, UK

ARTICLE INFO

Article history:
Received 7 June 2010
Received in revised form 11 August 2010
Accepted 15 August 2010
Available online 24 September 2010

Keywords:
Defects
Metal oxides
Ion transport
Diffusion
Molecular modelling

ABSTRACT

Ceria (CeO_2) and india (In_2O_3) represent two of the most important metal oxide systems for catalytic and optoelectronic applications, respectively. Here, we report analytical interatomic potential models for these two materials, which reproduce the materials structural, elastic and dielectric properties. The potential models are then applied to study the fundamental defect reactions occurring in these materials. Further, we focus on the mechanisms of oxygen diffusion through the lattice, arising from anion Frenkel-pair formation, which is of particular interest for understanding the processes involved in radiation damage and catalysis. The thermodynamic barriers associated with the formation of the first stable anion Frenkel-pairs are 5.80 eV and 4.81 eV in cerium dioxide and indium sesquioxide, respectively; while for recombination, we calculate barriers of 0.78 eV and 0.23 eV. The threshold displacement energy for radiation damage in ceria is found to be 35.4 eV, in excellent agreement with recent experimental measurements, while for india we predict a value of 14.2 eV.

1. Introduction

Metal oxides are employed in a diverse range of technological applications. Theoretical modelling of this class of material has proved successful, using both electronic structure and classical potential techniques, and has helped to increase our knowledge of the atomistic processes occurring in these complex systems, including defect processes in functional metal oxides, *e.g.* ZnO [1–3] and Al_2O_3 [4,5]. In this study, we address two important metal oxide systems: (i) india (In_2O_3), which is a wide band gap conductive metal oxide used as a transparent contact in solar cells and flat panel displays [6,7]; and (ii) ceria (CeO_2), which has found widespread use as an electrolyte in solid-oxide fuel cells and in three-way automobile exhaust catalysts due to its remarkable ability to support oxygen sub- and super-stoichiometry, thus acting as an oxygen buffer for redox reactions. Both materials have gathered interest for nuclear applications, including radiation detection and inert reactor lining [8–11], and CeO_2 has demonstrated potential for radiolytic production of H_2 from water [12].

There has been great interest in modelling the bulk, surface and defect properties of these two materials in the past, using both quantum and classical techniques [1,13–22]. In particular, Ágoston and Albe recently addressed ionic diffusion in india, using electronic structure techniques [19], while Guglielmetti et al. investigated the threshold energies for cerium and oxygen displacements in ceria by classical molecular dynamics [20]. In this study, we present robust interatomic potential models for these two systems, which reproduce their pertinent physicochemical properties. In addition to the fundamental defect reactions, the models are applied to investigate the barrier for interstitial oxygen diffusion arising from the creation of an anion Frenkel-pair, which may form under thermodynamic equilibrium or through non-equilibrium processes, such as radiation damage. The calculated thermodynamic barriers for the formation of the first stable anion Frenkel-pairs are 5.80 eV and 4.81 eV in CeO_2 and In_2O_3, respectively. Furthermore, the potential models that we have developed will be of value in subsequent investigations of these two important materials, in particular for performing hybrid QM/MM calculations [23,24].

2. Computational details

The interatomic potentials adopted are based on the Born model of the ionic solid [25]; ionic interactions are represented through pairwise Coulomb, and short-range Buckingham, Lennard–Jones and/or Morse potentials. In order to describe accurately the energetic and structural properties, electronic polarisation must be explicitly taken into account, which is achieved using the shell model [26,27]. In all cases, the sum of the core and shell charges is constrained to conserve the formal charge state of the ions. The potential models were derived by fitting parameters of interactions to reproduce the known material properties including high-pressure structural data and the low temperature phonon dispersion curves. The complete potential parameters can be found on our on-line interatomic potential database [28], and full details will be published elsewhere [13,29].

The defect calculations were performed within the embedded-cluster Mott–Littleton method [30], which describes an isolated defect centre in the true impurity limit (at infinite dilution). Within the

* Corresponding author.
E-mail address: a.walsh@ucl.ac.uk (A. Walsh).

0167-2738/$ – see front matter © 2010 Elsevier B.V. All rights reserved.
doi:10.1016/j.ssi.2010.08.010

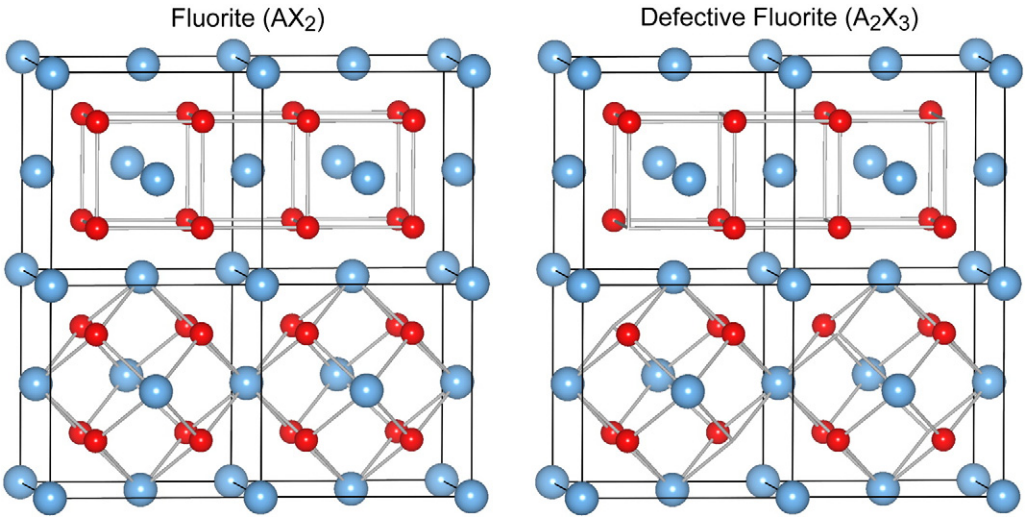

Fig. 1. (left panel) The fluorite crystal structure with lines connecting nearest neighbour oxygen ions drawn to emphasise their cubic arrangement, and connections between Ce and O ions drawn to emphasise the cage-like structure around the interstitial lattice site located at (1/2, 1/2, 1/2). (right panel) A defective fluorite structure, similar to bixbyite, with one quarter of the anion sites vacant. Blue is reserved for the cations (large balls), with red for oxygen (small balls).

Mott–Littleton method, the structural model is divided into an inner region centred around the defect, in which interactions are explicitly treated (region I), and an outer region, which is described via a linear response approach (region II). In our calculations, the radius of region I was chosen as 10 Å (>300 atoms) with a 25 Å radius for region IIa (>3000 atoms); the region IIb continuum commences outside these spheres and extends to infinity. These settings yield convergence of the defect energies to *ca.* 0.1 eV. It should be noted that the chemical potential of the individual ions is not directly known using classical pair potentials: the ion self-energy is defined as zero at infinite separation; therefore, only the formation energy of stoichiometry-preserving defects can be directly compared to experiment; whereas the effects of non-stoichiometry may be only treated through the use of an appropriate Born–Haber cycle [31]. All defect simulations were performed using the GULP code [32].

To gain an initial insight into the migration pathways, we have developed an automated procedure that generates the energy landscape across a pre-defined grid of points. Herein, an energy landscape defined on a $3N_x \times 3N_y \times 3N_z$ grid across a $3 \times 3 \times 3$ supercell is first generated and then analysed, using the code Bubble [33]. For example, to investigate the energy required to displace an oxygen ion from its lattice site in In_2O_3, the lattice energy is computed for each of $N_xN_yN_z$ lattice energies are computed; the initial structure in each calculation is that of the bulk, but with one chosen oxygen ion displaced to, and fixed at, each of the grid points in turn. The lattice energy and any structural relaxations are computed using the GULP code [32]. To set up and manage the input–output for GULP, we use our in-house code PREGULP [34]. In the present work: (a) the grid spacing is approximately 0.3 Å; (b) the lattice energy is set to an upper threshold if the grid point is within 1.2 Å of a lattice atom; (c) as well as the core of the migrating ion, atoms further than 3.0 Å from the lattice vacancy and 6.0 Å from the migrating oxygen ion are held fixed during a structural relaxation. The relaxation radii of 3.0 Å and 6.0 Å take into account the stronger relaxation around the interstitial centre and approach the limiting values that avoid relaxation of all ions in the supercell. To simulate purely electronic relaxations, all cores are held fixed, *i.e.* only shells representing the valence electrons are moved in order to minimise the lattice energy. Once the energy across the grid is known, this set of data is fed into the Bubble code, which locates local minima and saddle points on the three-dimensional landscape. Note that as the grid has a spacing of 0.3 Å, the data for local minima and saddle points are approximate and include effects of periodicity (interaction of defect periodic images), so they were subsequently refined before assigning final values to barriers. In particular, the location and energy values for saddle points were refined using an explicit transition state search (based on the eigenvector following approach) within the Mott–Littleton model. Estimations for the threshold displacement energy required for radiation damage were taken at the saddle points on the $3N_x \times 3N_y \times 3N_z$ grid, but including only electronic (shell) relaxation to take into account the high kinetic energy of the displaced ion relative to the surrounding lattice ions.

3. Results and discussions

3.1. Ceria and india potential models

The majority of the previously reported classical interatomic potential models for ceria were recently reviewed in two studies by Galea et al. [35] and Xu et al. [36], including the parameterisations of Butler et al. [37], Grimes and Catlow [38], Vyas et al. [17] and Gotte et al. [14]; however, none of these models have proved entirely satisfactory in offering a balanced description of the structural, dielectric, elastic and phonon properties. Hence, to achieve this balance, we introduced a more complex set of two-body interatomic potentials, which are a linear combination of widely used analytical functions. The parameterisation of the new potentials will be discussed elsewhere [29]. We note that with these potentials we can reliably reproduce a large number of physical properties, which is not at the expense of the deterioration of the migration barriers for elementary defects, *e.g.* a value of 0.55 eV for vacancy driven oxide

Table 1
Calculated and experimental material properties of bixbyite In_2O_3 and fluorite CeO_2: a is the cubic lattice constant, B is the bulk modulus, ε_0 and ε_∞ are the static and high frequency dielectric constants and c are the elastic constants.

Property	India experiment	India potential[13]	Ceria experiment	Ceria potential[27]
a (Å)	10.117[42]	10.121	5.411[43]	5.411
B (GPa)	194.24[44]	193.77	204[40]–236[45]	207.91
ε_0^{11}	8.9–9.5[46]	9.05	24.5[47]	24.22
ε_∞^{11}	4.0[46]	3.90	5.31[47]	5.31
c_{11} (GPa)		297.75	403[40]	405.29
c_{12} (GPa)		141.78	105[40]	109.22
c_{44} (GPa)		76.42	60[40]	64.37

Table 2
Calculated formation energies (eV per defect) for a range of intrinsic defects and defect pairs in bixbyite In_2O_3 and fluorite CeO_2 using the interatomic potentials presented in the present work. The lattice energy (eV per formula unit) used in the calculation of the interstitial and Schottky defect disorder is also listed.

Defect	Ceria	India
$V_O^{\bullet\bullet}$	12.91	20.99
$V_{Ce}^{////}/V_{In}^{///}$	94.41	49.92
$O_i^{//}$	−6.49	−14.61
$Ce_i^{\bullet\bullet\bullet\bullet}/In_i^{\bullet\bullet\bullet}$	−62.53	−36.21
Cation Frenkel-pair	15.94	6.85
Anion Frenkel-pair	3.21	3.19
Interstitial disorder	9.12	4.87
Schottky disorder	5.79	4.44
E[Lattice]	−102.87	−140.60

migration in ceria, compared to 0.53 eV from earlier simulations [37] and 0.52 eV from experiment [39].

The lattice properties of the *fcc* fluorite phase (as shown in Fig. 1) derived from our new potential model are compared to experiment in Table 1: the experimental lattice constant is reproduced and all other properties are found to be in good agreement with experiment. Furthermore, the gamma-point phonon frequencies of 276 cm^{-1} (T_{1u}) and 473 cm^{-1} (T_{2g}), with a longitudinal optical mode at 588 cm^{-1} (A_{1u}) compare well to the values of 273, 465 and 597 cm^{-1} derived from room temperature Raman scattering measurements on ceria single crystals [40]. Our calculations also reproduce the experimentally determined phonon dispersion properties.

For india, we have recently reported a revised potential model, which provides an accurate description of the bixbyite structure, in addition to a number of high-pressure denser sequioxide polymorphs [13] and india nanoclusters [22]. The *bcc* bixbyite mineral structure is in fact a superstructure of a defective fluorite lattice, with one quarter of the anion sites vacant in order to adapt to the stoichiometry of the sesquioxide compounds; a schematic of the relationship to fluorite is shown in Fig. 1. Importantly for defect calculations, the dielectric properties are in excellent agreement with experiment. It is interesting to note that in comparison to ceria, the high frequency dielectric constant is lower by 26%, while the static dielectric constant is lower by 63%, indicative of much stronger screening in ceria.

3.2. Intrinsic point-defect formation

We consider the four principal cases of intrinsic ionic disorder at infinite dilution: Schottky, interstitial, and anion and cation Frenkel-

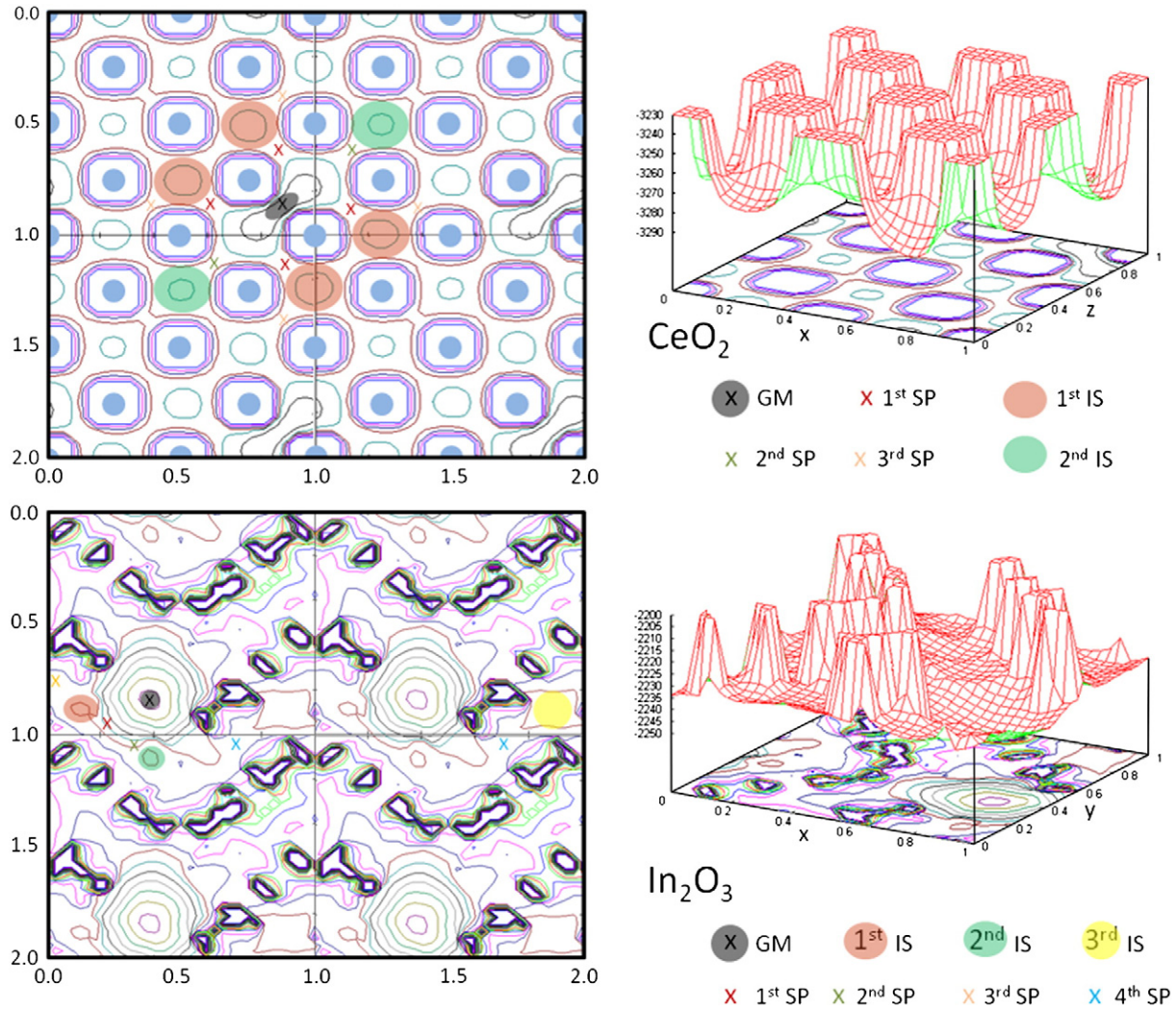

Fig. 2. Potential energy surfaces for anion Frenkel-pair formation in CeO_2 and In_2O_3. The surfaces were generated using a $2\times2\times2$ cubic supercell of fluorite ($1\times1\times1$ of bixbyite); a 2D slice through a (001) plane is shown in the left panel (for bixbyite the plot has been minimized with respect to total energy over a series of (001) planes at each grid point), with the corresponding energy profiles shown in the right panel. The oxygen vacancy site is shaded black (global minimum – GM), with coloured x's labeling the saddle points (SP) leading to the first stable interstitial site (IS) for Frenkel-pair formation. The axis labels represent fractional coordinates of the original fluorite unit cell.

pair formation. The Schottky defect represents the removal of cations and anions in stoichiometric units to form vacant lattice sites,

$$2In_{In} + 3O_O \rightleftharpoons 2V_{In}^{'''} + 3V_O^{\bullet\bullet} + In_2O_3(s)$$

$$Ce_{Ce} + 2O_O \rightleftharpoons V_{Ce}^{''''} + 2V_O^{\bullet\bullet} + CeO_2(s)$$

The associated Schottky defect energy is defined with respect to isolated ion removal and the addition of one formula unit to the bulk lattice:

$$E_{Schottky}^{In_2O_3} = \frac{1}{5}\left(2E[V_{In}^{'''}] + 3E[V_O^{\bullet\bullet}] + E[In_2O_3]\right)$$

$$E_{Schottky}^{CeO_2} = \frac{1}{3}\left(E[V_{Ce}^{''''}] + 2E[V_O^{\bullet\bullet}] + E[CeO_2]\right)$$

Correspondingly, interstitial disorder can occur through the formation of one formula unit of interstitial sites:

$$E_{Interstitial}^{CeO_2} = \frac{1}{3}\left(E[Ce_i^{\bullet\bullet\bullet\bullet}] + 2E[O_i^{''}] - E[CeO_2]\right)$$

$$E_{Interstitial}^{In_2O_3} = \frac{1}{5}\left(2E[In_i^{\bullet\bullet\bullet}] + 3E[O_i^{''}] - E[In_2O_3]\right)$$

Finally, a Frenkel defect is created by the displacement of an occupied lattice ion onto an interstitial position, *e.g.*

$$O_O \rightleftharpoons O_i^{''} + V_O^{\bullet\bullet}$$

for the anion Frenkel-pair, with a formation energy calculated from:

$$E_{Frenkel} = \frac{1}{2}\left(E[O_i^{''}] + E[V_O^{\bullet\bullet}]\right).$$

The defect reaction energies are listed in Table 2 for both india and ceria. In both cases anion Frenkel-pair formation is the most favourable form of intrinsic ionic disorder, with an associated energy of 3.2 eV per defect in both materials. In comparison, cation Frenkel-pair formation is much higher in energy, owing to the increased cationic charges. The energetic cost of both Schottky and interstitial disorder is greater than 4 eV per defect.

3.3. Anion Frenkel-pair formation

As anion Frenkel-pair formation has been identified as the most feasible defect reaction, which can also occur when an oxygen atom is displaced from its lattice site by high energy radiation, we will explore the formation process in more detail.

In fluorite structured CeO_2, a local anion Frenkel-pair consisting of a vacancy at (1/4, 1/4, 1/4) and interstitial at (1/2, 1/2, 1/2) is unstable with respect to recombination, hence, the first stable pair contains the interstitial in the next-nearest position at a separation of 4.49 Å. The defect formation energy is 2.51 eV per defect, yielding a binding energy of 1.40 eV relative to the non-interacting pair, which arises from the Coulombic attraction between the two oppositely charged defect centres. In bixbyite structured In_2O_3, the closest stable bound pair consists of the vacancy and interstitial separated by a distance of *ca.* 3.75 Å in the <110> direction. A formation energy of 2.29 eV is calculated per defect, yielding a strong binding energy of 1.80 eV, consistent with the lower dielectric constant of india relative to ceria, which results in a weaker screening of the electrostatic interactions.

The potential energy surfaces associated with oxygen migration from its lattice site in both materials are shown in Fig. 2. Due to its high crystal symmetry, the migration pathways observed for ceria are relatively straightforward: local minima are found where the migrating oxygen ion occupies one of the fluorite regular interstitial sites, while barriers are present where it is forced to cross between the interstitial sites. A number of possible transition state structures have previously been identified for ion migration within the fluorite structure [37,41], which are all plausible mechanisms for oxygen transport in the bulk material. In contrast to the well-defined array of regular interstitial sites in the fluorite structure, the nature of the migration process in bixbyite is more complex. Migration of an oxygen ion from its lattice site does not occur within a single lattice plane, but involves hopping between adjacent planes, the details of which will be given elsewhere. Instead, we will focus on the first barrier determining the formation of a stable anion Frenkel-pair, *i.e.* the vacancy–interstitial pairs previously identified.

The energy cost associated with forming the first stable anion Frenkel-pair in ceria and india is 5.02 eV and 4.58 eV, respectively. However, formation of these bound pairs is an activated process, with the corresponding saddle point locations highlighted in Fig. 2. An explicit transition state search around these points reveals barriers of 5.80 eV and 4.81 eV respectively, with respect to the oxygen ion at its ideal lattice site. Conversely, the barriers for Frenkel-pair recombination are small, 0.78 eV and 0.23 eV, which is representative of the strong (poorly screened) Coulomb attraction. The resultant energy landscape along with relevant reaction energies are sketched in Fig. 3. While the identified local minimum should be stable in ceria at finite temperatures, significant thermal recombination rates would be expected to occur in india owing to the low barrier. Bound pairs, stable at elevated temperatures, would only be expected to occur in india for the next-nearest neighbour vacancy–interstitial pairs, which has the implication that the material should be less susceptible to irreversible damage in a radiation environment.

Finally, investigation of the threshold displacement energies for radiation damage reveals values of 35.4 eV and 14.2 eV for ceria and

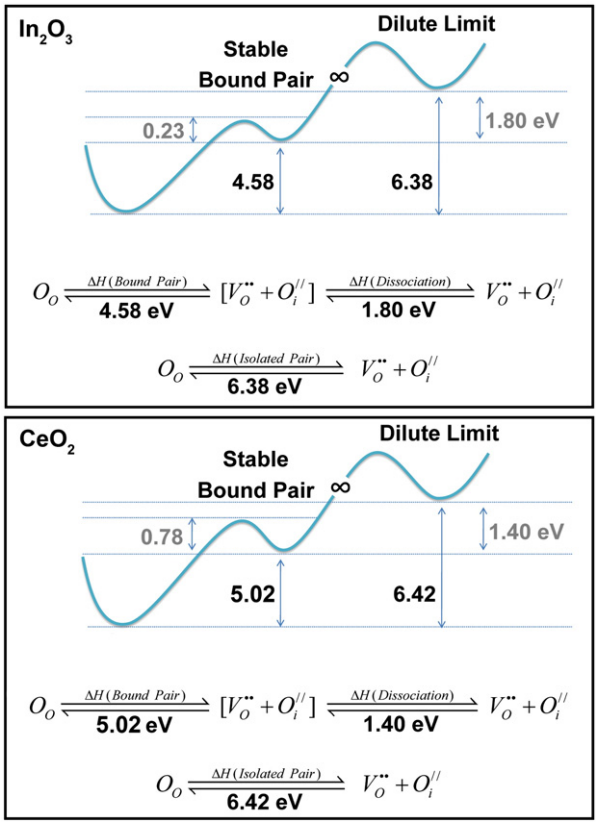

Fig. 3. Schematic reaction pathways for anion Frenkel-pair formation in india (upper panel) and ceria (lower panel) using our calculated reaction energies (in eV per defect pair) and thermodynamic barriers.

india, respectively, using the Bubble code. Further refinement of the grid would result in somewhat smaller values, which compares favourably with recent experimental data for ceria of 25–33 eV [48], and is consistent with previous estimations of 27 eV [20] from classical molecular dynamics simulations. Our estimation for india is the first to be reported, to our knowledge, and future experimental verification would be welcome.

4. Conclusion

We have reported robust interatomic potential models for CeO_2 and In_2O_3, which reproduce the structural and physical properties of the thermodynamically stable phases. We have presented results of the potential models applied to fundamental defect reactions in these materials, including the barriers associated with anion Frenkel-pair formation. Both materials exhibit similar formation energies for the generation of isolated Frenkel-pairs, with thermodynamic barriers for the formation of the first stable bound pairs being 5.80 eV and 4.81 eV in ceria and india, respectively. While this study offers initial insights into the complex potential energy landscape for Frenkel-pair formation and ion transport in these materials, we are currently investigating approaches to explore the ionic diffusion mechanism using a combination of classical and quantum chemical (QM/MM) approaches, which would shed light on issues relating to ion transport, conductivity and the redox chemistry.

Acknowledgements

The authors acknowledge support by an EPSRC Portfolio Partnership (Grant no. ED/D504872) and membership of the UK's HPC Materials Chemistry Consortium, which is funded by EPSRC (Grant no. EP/F067496). A.W. would like to acknowledge funding from a Marie-Curie Intra-European Fellowship from the European Union under the Seventh Framework Programme.

References

[1] C.R.A. Catlow, Z.X. Guo, M. Miskufova, S.A. Shevlin, A.G.H. Smith, A.A. Sokol, A. Walsh, D.J. Wilson, S.M. Woodley, Proc. R. Soc. A 368 (1923) (2010) 3379.
[2] C.R.A. Catlow, S.A. French, A.A. Sokol, A.A. Al-Sunaidi, S.M. Woodley, J. Comput. Chem. 29 (13) (2008) 2234.
[3] A.A. Sokol, S.A. French, S.T. Bromley, C.R.A. Catlow, H.J.J.v. Dam, P. Sherwood, Faraday Discuss. 134 (2007) 267.
[4] C.R.A. Catlow, R. James, W.C. Mackrodt, R.F. Stewart, Phys. Rev. B 25 (2) (1982) 1006.
[5] A.A. Sokol, A. Walsh, C.R.A. Catlow, Chem. Phys. Lett. 492 (2010) 44.
[6] A. Walsh, J.L.F. Da Silva, S.-H. Wei, C. Korber, A. Klein, L.F.J. Piper, A. DeMasi, K.E. Smith, G. Panaccione, P. Torelli, D.J. Payne, A. Bourlange, R.G. Egdell, Phys. Rev. Lett. 100 (16) (2008) 167402.
[7] P.P. Edwards, A. Porch, M.O. Jones, D.V. Morgan, R.M. Perks, Dalton Trans. 19 (2004) 2995.
[8] K. Arshak, O. Korostynska, IEEE Sensors 3 (2006) 717.
[9] W.J. Weber, Radiat. Eff. 83 (1) (1984) 145.
[10] K. Arshak, O. Korostynska, Iee Proc. Circ. Devices Syst. 150 (4) (2003) 361.
[11] M. Burghartz, H. Matzke, C. Leger, G. Vambenepe, M. Rome, J. Alloys Compd. 271 (1998) 544.
[12] J.A. LaVerne, L. Tandon, J. Phys. Chem. B 106 (2) (2002) 380.
[13] A. Walsh, C.R.A. Catlow, A.A. Sokol, S.M. Woodley, Chem. Mater. 21 (20) (2009) 4962.
[14] A. Gotte, D. Spångberg, K. Hermansson, M. Baudin, Solid State Ionics 178 (25–26) (2007) 1421.
[15] M. Nolan, S. Grigoleit, D.C. Sayle, S.C. Parker, G.W. Watson, Surf. Sci. 576 (1–3) (2005) 217.
[16] L. Minervini, M.O. Zacate, R.W. Grimes, Solid State Ionics 116 (3–4) (1999) 339.
[17] S. Vyas, R.W. Grimes, D.H. Gay, A.L. Rohl, J. Chem. Soc. Faraday Trans. 94 (3) (1998) 427.
[18] P. Agoston, K. Albe, Phys. Chem. Chem. Phys. 11 (17) (2009) 3226.
[19] P. Ágoston, K. Albe, Phys. Rev. B 81 (19) (2010) 195205.
[20] A. Guglielmetti, A. Chartier, L.v. Brutzel, J.-P. Crocombette, K. Yasuda, C. Meis, S. Matsumura, Nucl. Instrum. Methods B 24 (2008) 5120.
[21] J.L.F. Da Silva, M.V. Ganduglia-Pirovano, J. Sauer, V. Bayer, G. Kresse, Phys. Rev. B 75 (4) (2007) 045121.
[22] A. Walsh, S.M. Woodley, Phys. Chem. Chem. Phys. 12 (30) (2010) 8446.
[23] A.A. Sokol, S.T. Bromley, S.A. French, C.R.A. Catlow, P. Sherwood, Int. J. Quantum Chem. 99 (5) (2004) 695.
[24] P. Sherwood, A.H. de Vries, M.F. Guest, G. Schreckenbach, C.R.A. Catlow, S.A. French, A.A. Sokol, S.T. Bromley, W. Thiel, A.J. Turner, S. Billeter, F. Terstegen, S. Thiel, J. Kendrick, S.C. Rogers, J. Casci, M. Watson, F. King, E. Karlsen, M. Sjøvoll, A. Fahmi, A. Schäfer, C. Lennartz, J. Mol. Struct. 632 (1–3) (2003) 1.
[25] M. Born, K. Huang, Dynamical Theory of Crystal Lattices, Oxford University Press, Oxford, 1956.
[26] B.G. Dick, A.W. Overhauser, Phys. Rev. 112 (1) (1958) 90.
[27] G.V. Lewis, C.R.A. Catlow, J. Phys. Condens. Matter 18 (6) (1985) 1149.
[28] UCL Materials Chemistry Interatomic Potential Database: http://www.ucl.ac.uk/klmc/Potentials.
[29] A.A. Sokol et al., In Preparation (2010).
[30] N.F. Mott, M.J. Littleton, Trans. Faraday Soc. 34 (1938) 485.
[31] C.M. Freeman, C.R.A. Catlow, J. Solid State Chem. 85 (1) (1990) 65.
[32] J.D. Gale, A.L. Rohl, Mol. Simul. 29 (5) (2003) 291.
[33] S.M. Woodley, A.M. Walker, Mol. Simul. 33 (15) (2007) 1229.
[34] S.M. Woodley, G. Maurin, (unpublished).
[35] N.M. Galea, D.O. Scanlon, P. Martin, G.W. Watson, P. Sherwood, J. Surf. Sci. Nanotechnol. 7 (2009) 413.
[36] H. Xu, R.K. Behera, Y. Wang, F. Ebrahimi, S.B. Sinnott, E.D. Wachsman, S.R. Phillpot, Solid State Ionics 181 (11–12) (2010) 551.
[37] V. Butler, C.R.A. Catlow, B.E.F. Fender, J.H. Harding, Solid State Ionics 8 (2) (1983) 109.
[38] R.W. Grimes, C.R.A. Catlow, Philos. Trans. R. Soc. A 335 (1639) (1991) 609.
[39] B.C.H. Steele, J.M. Floyd, Proc. Br. Ceram. Trans. 72 (1971) 55.
[40] A. Nakajima, A. Yoshihara, M. Ishigame, Phys. Rev. B 50 (18) (1994) 13297.
[41] C.R.A. Catlow, M.J. Norgett, T.A. Ross, J. Phys. C 10 (10) (1977) 1627.
[42] M. Marezio, Acta Crystallogr. 20 (6) (1966) 723.
[43] J.D. McCullough, J. Am. Chem. Soc. 72 (1950) 1386.
[44] D. Liu, W.W. Lei, B. Zou, S.D. Yu, J. Hao, K. Wang, B.B. Liu, Q.L. Cui, G.T. Zou, J. Appl. Phys. 104 (8) (2008) 083506.
[45] L. Gerward, J.S. Olsen, Powder Diffr. 8 (1993) 127.
[46] I. Hamberg, C.G. Granqvist, J. Appl. Phys. 60 (11) (1986) R123.
[47] S. Mochizuki, Phys. Status Solidi B 114 (1) (1982) 189.
[48] K. Yasunaga, K. Yasuda, T. Matsumura, K. Sonoda, Nucl. Instrum. Methods B 266 (2008) 2877.